Nuclear–Electronic Orbital Time-Dependent Configuration Interaction Method

Scott M. Garner,[†] Shiv Upadhyay,[‡] Xiaosong Li,[*,‡] and Sharon Hammes-Schiffer[*,†]

[†]*Department of Chemistry, Princeton University, Princeton NJ 08544, United States*

[‡]*Department of Chemistry, University of Washington, Seattle WA 98195, United States*

E-mail: xsli@uw.edu; shs566@princeton.edu

Abstract

Combining real-time electronic structure with the nuclear–electronic orbital (NEO) method has enabled the simulation of complex nonadiabatic chemical processes. However, accurate descriptions of hydrogen tunneling and double excitations require multiconfigurational treatments. Herein, we develop and implement the real-time NEO time-dependent configuration interaction (NEO-TDCI) approach. Comparison to NEO-full CI calculations of absorption spectra for a molecular system shows that the NEO-TDCI approach can accurately capture the tunneling splitting associated with the electronic ground state as well as vibronic progressions corresponding to double electron-proton excitations associated with excited electronic states. Both these features are absent from spectra obtained with single reference real-time NEO methods. Our simulations of the hydrogen tunneling dynamics illustrate the oscillation of the proton density from one side to the other via a delocalized, bilobal proton wavefunction. These results indicate that the NEO-TDCI approach is highly suitable for studying hydrogen tunneling and other inherently multiconfigurational systems.

TOC Graphic

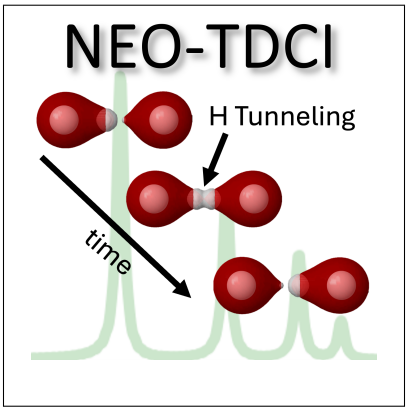

Real-time electronic structure methods are a natural tool for studying ultrafast chemical dynamics and molecular responses to external perturbations.[1–3] Real-time methods have additionally proven to be incredibly powerful for calculating absorption spectra, especially for spectra with densely packed excited states where time-independent methods struggle.[4] By evolving multicomponent wavefunctions, where more than one type of particle is treated quantum mechanically,[5–11] real-time theory is capable of simulating additional interesting physical phenomena. In particular, combining the nuclear–electronic orbital (NEO) framework, which treats electrons and nuclei on equal footing,[7,10,11] with real-time theory enables the calculation of vibrational spectra,[12,13] as well as the simulation of photoinduced proton transfer[12,14–16] and plasmon-induced dissociation[17] reactions.

The most common real-time theory is real-time time-dependent density functional theory (RT-TDDFT) due to its reasonably high accuracy at relatively low computational cost.[1–3,18,19] There are, however, many well-documented chemical motifs where RT-TDDFT and DFT struggle to produce accurate predictions.[20] Charge transfer states, Rydberg excitations, and systems with inherently multiconfigurational nature all pose challenges to RT-TDDFT.[2] It is possible to address some of these challenges within the RT-TDDFT framework. For example, optimally tuned range-separated hybrid functionals can produce accurate descriptions of charge transfer states.[21] However, some issues, notably states with multiconfigurational character, where a single Slater determinant is an insufficient reference, remain incompatible within the typical RT-TDDFT framework.

An alternative approach is time-dependent configuration interaction (TDCI), which rather than propagating the total density of a single Slater determinant instead propagates time-dependent coefficients of a CI expansion.[2,22,23] Because the computational cost of the exact full CI (FCI) solution scales exponentially with system size, practical TDCI methods either truncate the allowed excitation level[24–31] or limit the orbitals in which excitations are considered in active space treatments.[23,32–36] Time-dependent complete active space CI (TD-CASCI) theory is capable of describing strong correlation and multiply excited states

provided the proper orbitals are included in the active space. Within the NEO framework, multiconfigurational approaches are essential for describing the bilobal proton densities characteristic of hydrogen tunneling systems.[7,37] A variety of time-independent multiconfigurational NEO methods have been developed, including NEO multiconfigurational self-consistent field (NEO-MCSCF),[7,37,38] multistate DFT (NEO-MSDFT),[39,40] selected CI (NEO-SCI),[41,42] and density matrix renormalization group (NEO-DMRG).[43,44]

In this work, we implement real-time NEO time-dependent CI (NEO-TDCI) theory and demonstrate its effectiveness for studying multiconfigurational protonic systems. We provide data showing how spectra calculated from a single NEO-TDCI simulation can capture tunneling splittings and vibronic progressions, both of which cannot be captured by single reference theories such as RT-NEO-TDDFT and the time-dependent Hartree-Fock variant, RT-NEO-TDHF. Furthermore, we highlight the advantages of NEO-TDCI over time-independent methods, particularly for calculating spectra with a high density of vibronic transitions. Finally, we show how NEO-TDCI can be used to study proton tunneling dynamics for a model system in which the proton moves on a double-well potential energy surface within the conventional electronic structure framework but oscillates back and forth within the NEO framework.

The NEO-TDCI wavefunction is constructed as a linear combination of multicomponent states:

$$|\Psi(t)\rangle = \sum_{i,j} c_{ij}(t) \, |\Phi_i^{\mathrm{e}}\rangle \, \left|\Phi_j^{\mathrm{p}}\right\rangle \tag{1}$$

where $|\Phi_i^{\mathrm{e}}\rangle$ and $\left|\Phi_j^{\mathrm{p}}\right\rangle$ are individual electronic and protonic Slater determinants, respectively. Each individual Slater determinant is constructed from time-independent electronic or protonic molecular orbitals determined by a NEO-HF calculation. For this work, we utilize a complete active space for both electrons and protons, although in principle any multideterminant NEO expansion may be used.

The time-dependent wavefunction is represented in this basis of time-independent product

states by the expansion coefficients, $\mathbf{c}(t)$. The real-time propagation is carried out using a symplectic split operator (SSO) integrator.[45,46] We briefly summarize the algorithm here with the necessary modifications for NEO-TDCI. For the SSO method, the time-dependent coefficients may be split into real and imaginary components:

$$\mathbf{c}(t) = \mathbf{p}(t) + i\mathbf{q}(t), \tag{2}$$

The time propagation for each component can be carried out independently in a leap frog fashion:

$$\frac{d\mathbf{q}(t)}{dt} = -\mathcal{H}(t)\mathbf{p}(t), \tag{3}$$

$$\mathbf{q}(t + 0.5\Delta t) = \mathbf{q}(t - 0.5\Delta t) + \Delta t \frac{d\mathbf{q}(t)}{dt}, \tag{4}$$

$$\frac{d\mathbf{p}(t + 0.5\Delta t)}{dt} = \mathcal{H}(t + 0.5\Delta t)\mathbf{q}(t + 0.5\Delta t), \tag{5}$$

$$\mathbf{p}(t + \Delta t) = \mathbf{p}(t) + \Delta t \frac{d\mathbf{p}(t + 0.5\Delta t)}{dt}. \tag{6}$$

where $\mathcal{H}(t)$ is the time-dependent NEO-CI Hamiltonian, which includes the kinetic energies of the electrons and quantum protons, all Coulomb interactions among the electrons, quantum protons, and classical nuclei, and any time-dependent external fields. For our purposes, the only time dependence in $\mathcal{H}(t)$ comes from a time-dependent applied electric field. Additional details regarding the propagation algorithm can be found in the Supporting Information.

The key difference between NEO-TDCI and TDCI is in the implementation of the matrix-vector products $\mathcal{H}(t)\mathbf{p}(t)$ and $\mathcal{H}(t)\mathbf{q}(t)$ used to form the time derivatives. We have implemented the NEO-TDCI and NEO-CASCI methods in a modified version of Chronus Quantum.[47] Our NEO-CASCI implementation utilizes a generalized version of a standard direct CI algorithm[48] to account for the multicomponent wavefunction in the matrix-vector product. The details of the NEO-CI Hamiltonian are readily available in previous work.[7]

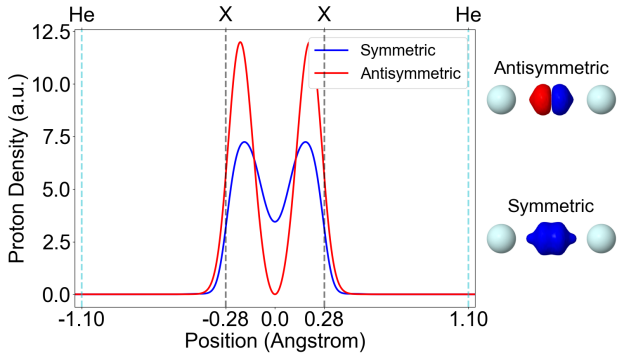

Figure 1: One-dimensional slices of the proton density along the He–He axis (left) and approximate three-dimensional proton wavefunctions (right) of $HeHHe^+$ for the two lowest energy vibronic states, labeled symmetric and antisymmetric, computed with the NEO-FCI method. The energy splitting between these two vibronic states corresponds to the hydrogen tunneling splitting associated with the ground electronic state. The dashed vertical lines denote the location of the helium atoms (solid cyan) as well as the centers of the protonic (and associated electronic) basis functions (dashed black). The proton wavefunction plots show the primary occupied natural orbital for each of these lowest two energy NEO-FCI vibronic states. In both states, the orbital shown accounts for $> 98.3\%$ of the wavefunction. The three dimensional plotting is done with Jmol[49] with isosurface value 0.05.

Our model system is the $HeHHe^+$ molecular ion at a He–He distance of 2.2 Å, where the hydrogen moves on a double-well potential energy surface within the conventional electronic structure framework.[50] This system is small enough to allow benchmarking against the time-independent NEO-FCI solution, yet still exhibits proton tunneling in the vibronic ground state. All calculations in the main text use the 6-31G electronic[51] and PB4-D[52] protonic basis sets and represent the hydrogen with two basis function centers containing both electronic and protonic basis functions. We perform NEO-TDCI simulations using (4e,8o)/(1p,46o) (4 electrons in 8 orbitals, 1 proton in 46 orbitals) active spaces, which in this case is equivalent to a NEO-FCI calculation.

We first calculate the absorption spectra of $HeHHe^+$. As we are able to afford NEO-FCI calculations, we also diagonalize the NEO-FCI Hamiltonian matrix and calculate the vibronic excitation energies and oscillator strengths relative to the ground vibronic state as our benchmark exact answer for the fixed heavy atom geometry and basis sets used. Visualizations of the proton density and approximate proton wavefunctions for the two lowest

energy vibronic states, which showcase the hydrogen tunneling behavior, are shown in Figure 1. Quantitative comparison to experimental references will require larger and more accurate electronic and protonic basis sets and therefore truncated active spaces. Exactly how to to define an effective multicomponent active space is still an active area of research[38] and is beyond the scope of this work. Nevertheless, the basis sets used here provide enough flexibility to gain a qualitative understanding of the new insights NEO-TDCI can provide over single reference real-time NEO methods.

The initial wavefunction for the NEO-TDCI simulation is the NEO-FCI ground state, where the proton is represented by a bilobal wavefunction delocalized between the two He nuclei (symmetric proton wavefunction in Figure 1). In the conventional Born-Oppenheimer electronic structure framework, the proton is moving on a symmetric double-well potential energy surface, and the bilobal proton wavefunction corresponds to equal density in both potential wells. We also perform RT-NEO-TDHF and RT-NEO-TDDFT simulations starting from their respective broken symmetry SCF solutions (i.e., the proton density is localized in one of the potential wells).[37] For calculating absorption spectra, the initial wavefunctions are perturbed with a delta pulse electric field polarized along one of the principal axes. Complete simulation details are provided in the Supporting Information.

Figure 2 shows the oscillations of the protonic and electronic dipole moments along the He–He axis. The most striking difference among the three methods is the low-frequency oscillation in the NEO-TDCI protonic dipole moment that is absent in the RT-NEO-TDDFT and RT-NEO-TDHF protonic dipole moments. This primary low-frequency mode is associated with the tunneling splitting between the two lowest energy NEO-CI solutions, which correspond to delocalized, bilobal symmetric and antisymmetric proton wavefunctions (Figure 1). In contrast, the primary mode in the single reference theories is at much higher frequency, corresponding to more localized proton densities discussed further below. Similar to the protonic component, the electronic dipole moment calculated with NEO-TDCI clearly is modulated by more lower-frequency components than is the electronic dipole moment cal-

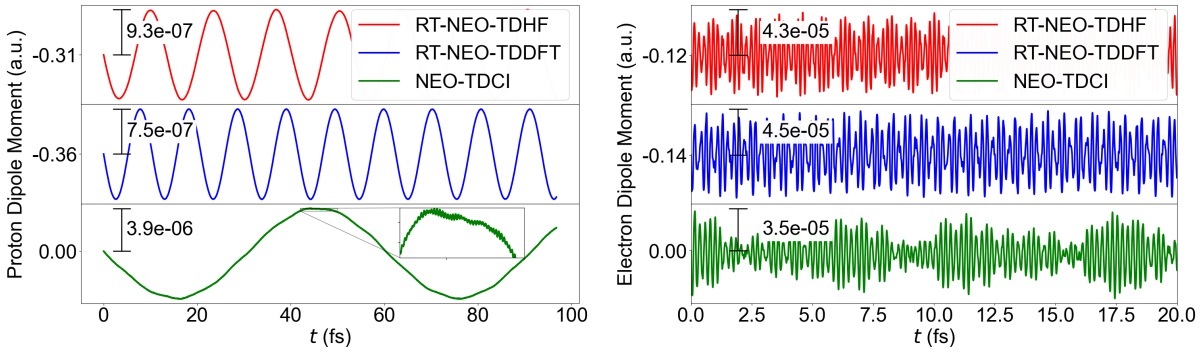

Figure 2: Time-dependent dipole moments along the He–He axis in the $HeHHe^+$ system for both the protonic (left) and electronic (right) components. The magnitude of the equilibrium dipole moment is indicated on each panel, and the magnitude of the oscillations about this value is shown for each method. The inset on the protonic NEO-TDCI panel shows high-frequency oscillations of the protonic dipole moment. Note that the protonic dipole moment is plotted over almost 100 fs, while the electronic dipole moment is only plotted over the first 20 fs of the same simulation.

culated with either RT-NEO-TDDFT or RT-NEO-TDHF.

The spectra resulting from the Fourier transform of the total dipole moment, including both electronic and protonic dipole moment contributions, are shown in Figure 3. Details of the Fourier transform are included in the Supporting Information. Although the complete real-time spectra are each generated from a single Fourier transform of the dipole moment, for clarity we plot two different regions: the left panel shows vibrational frequencies arising from primarily protonic excitations, while the right panel shows the much higher energy electronic excitations. The NEO-FCI stick spectra are plotted as a benchmark.

We start by inspecting the vibrational excitation region, shown in the left panel of Figure 3. For $HeHHe^+$, there are four vibrational modes, but with fixed helium nuclei only three modes are active: the degenerate off-axis bending mode and the on-axis tunneling splitting mode. The degenerate bending frequency is at 3447 cm^{-1} , while the NEO-FCI tunneling splitting is at 552 cm^{-1} . Relative to the time-independent NEO-FCI reference, all three time-dependent methods somewhat accurately reproduce the bending frequency, but only NEO-TDCI accurately predicts the lower energy tunneling splitting between the symmetric and antisymmetric bilobal proton vibrational wavefunctions. Both RT-NEO-TDDFT and

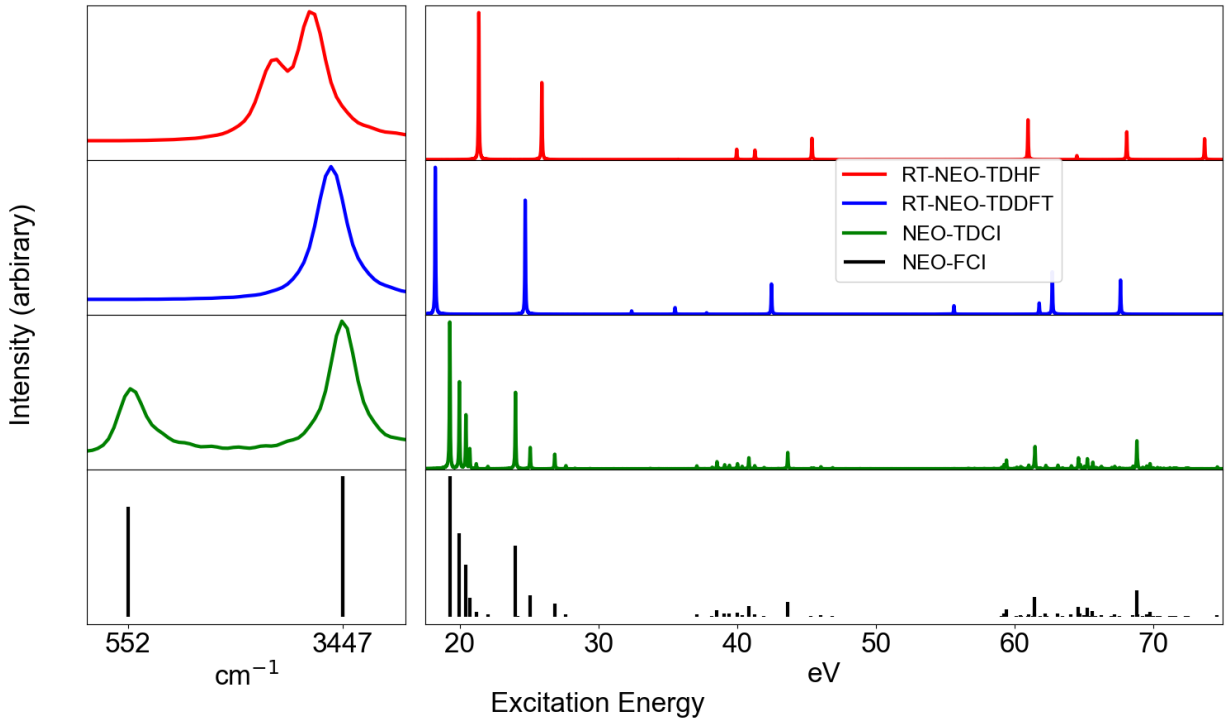

Figure 3: Calculated spectra of $HeHHe^+$. The left panel shows the fundamental vibrational excitations. The right panel horizontal axis starts at the lowest calculated electronic excitation and shows a portion of each total spectrum.

RT-NEO-TDHF predict the on-axis hydrogen vibrational mode at much too high of an energy. For RT-NEO-TDDFT, it is almost degenerate with the bending mode and therefore not obviously seen in the spectrum. Because these single reference theories break symmetry and localize the proton near one He nucleus, they are likely capturing the first vibrational excitation along the He–He axis corresponding to a He–H stretch mode rather than the energy difference associated with the hydrogen tunneling splitting.

Focusing on the electronic excitation energy range in the right panel of Figure 3, it is clear that while the single reference theories capture the major excitations present in the NEO-FCI spectrum, they miss the majority of the finer details in the structure of the NEO-FCI spectrum that NEO-TDCI captures. This observation is not surprising, in that RT-NEO-TDDFT and RT-NEO-TDHF are limited to describing single excitations, whereas NEO-FCI and NEO-TDCI contain all possible excitations in the active space, including double excitations. Although some excitations are double electronic excitations, the NEO approach also enables us to capture doubly excited states corresponding to simultaneous electronic and protonic excitations.

For a clear example of simultaneous electronic and protonic excitations, we focus on the first progression of excited vibronic states located around 20 eV. A focused view of this region computed with the NEO-TDCI and NEO-FCI methods is given in Figure 4 (left). The single reference theories are omitted because they feature a single peak without any additional structure, as can be seen in Figure 3. The excited vibronic states shown in Figure 4 (left) correspond to the vibronic progression on the excited electronic surface. To illustrate this point, we plot one-dimensional slices of both the electron and proton densities along the He–He axis for the NEO-FCI vibronic states producing this progression. We use the time-independent NEO-FCI densities because they are simple to isolate for analysis. The time-dependent wavefunction propagated in the NEO-TDCI simulation is a linear combination containing these adiabatic vibronic states, but they are difficult to extract individually.

For all states labeled A–E, the excited state electron density is almost identical, indicating

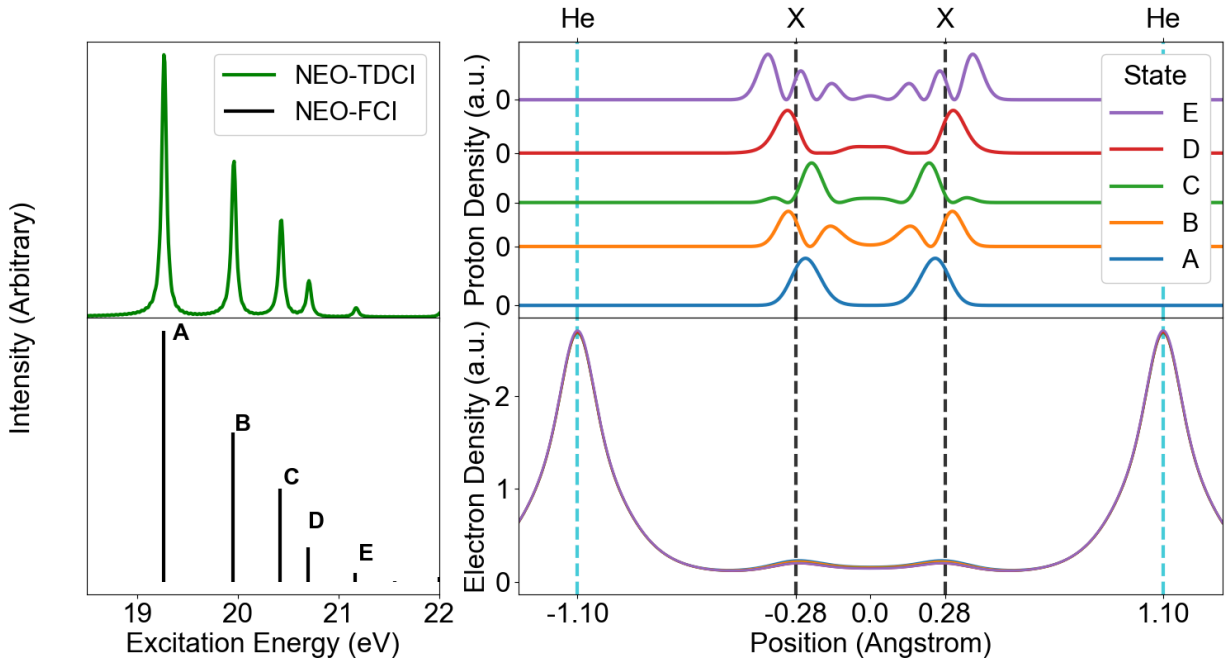

Figure 4: Calculated spectra of $HeHHe^+$ in a focused region illustrating a vibronic progression. The left panel is extracted from the lower two panels on the right side of Figure 3. The right panel shows one-dimensional slices of the electron and proton densities along the He–He axis for the vibronic states associated with the first singlet electronic excited state, as obtained from a time-independent NEO-FCI calculation. The dashed vertical lines denote the location of the helium atoms (solid cyan) as well as the centers of the protonic (and associated electronic) basis functions (dashed black). The electronic densities for all states are plotted on top of one another to show the same electronic character for all states (lower right panel), whereas the proton densities are offset vertically for clarity (upper right panel) with the zero density baseline indicated for each state. The ground vibronic state densities are shown in Figure S1 for comparison. Only the symmetry allowed vibronic states are shown here, whereas both symmetry allowed and symmetry forbidden vibronic states are shown in Figure S2.

that all vibronic states are associated with the same electronic state. The only very minor differences between the electron density are in the region along the He–He axis near the delocalized proton. The proton density shows the clear vibronic progression with increasing number of nodes in the vibrational wavefunction as the state energy increases from A to E. States A, B, and E form a clear progression of increasing level of vibrational excitation, indicated by an increase in the number of nodes on both sides (i.e., the two potential energy wells on the Born-Oppenheimer electronic excited state surface). The states labeled C and D are particularly interesting in that they exhibit proton density at the midpoint between the two helium atoms, where a potential energy barrier likely exists on the Born-Oppenheimer electronic excited state surface. For these states, the excited vibrational energy most likely exceeds that of the potential energy barrier.

State A is the ground vibrational state on the first singlet electronic excited state. The first ten vibrational states on this excited electronic state are shown in Figure S2. Similar to the ground electronic state, the proton moves on a double-well excited electronic state potential energy surface in conventional electronic structure theory. Although there is an antisymmetric bilobal proton vibrational wavefunction associated with a tunneling splitting for the excited electronic state within the NEO framework, transitions between vibronic states of different symmetries in the ground and first excited electronic states are prohibited by dipole selection rules. As such it does not show up in either the NEO-FCI or the NEO-TDCI spectra. Figure S2 shows the proton density for all vibronic states associated with the first singlet electronic excited state and discusses these symmetry considerations.

Furthermore, analogous simulations utilizing the larger cc-pVDZ electronic[53] and PB5-F protonic[52] basis sets, as well as additional simulations of the absorption spectra of the significantly larger FHF^- molecule, with active spaces are provided in the Supporting Information. For these larger calculations, our analysis shows that the NEO-TDCI method reproduces the low energy features of a time-independent NEO-CASCI calculation in an equivalent active space. Additionally, the NEO-TDCI method captures high energy features

that become computationally challenging to obtain in a time-independent framework.

Beyond calculating spectra, an important capability of the TDCI method is the simulation of nonequilibrium, real-time dynamics.[2,46] The quantization of the protonic wavefunction in the NEO-TDCI method enables the simulation of proton tunneling dynamics. In contrast to the spectra calculations, where charge oscillations are induced by perturbing the NEO-CI ground state with a delta pulse electric field, we now induce the dynamics via the construction of a nonequilibrium initial wavefunction. Similar tactics of manipulating the initial wavefunction have been used with RT-NEO-TDDFT to study proton transfer, typically via swapping the highest occupied and lowest unoccupied molecular orbitals (i.e., HOMO and LUMO) to model electronic photoexcitation.[12,14] For the application of NEO-TDCI to the $HeHHe^+$ system, we construct the initial wavefunction as a linear combination of NEO-CI states, i.e., a coherent superposition state. A natural advantage of constructing the initial state in this way is that in the absence of a perturbing field, the dynamics are purely dictated by the action of the Hamiltonian on its stationary states. In other words, in the absence of a perturbing field, all dynamics are controlled by interference patterns of complex phase factors associated with the Hamiltonian eigenstates. NEO-TDCI dynamics simulations constructed in this manner therefore reduce to solving a textbook quantum mechanics problem of evolving complex time-dependent coefficients associated with Hamiltonian eigenstates.

For systems in which the proton moves on a double-well potential energy surface within the conventional electronic structure framework, two natural orthonormal bases exist. These two bases are the basis of localized states in either well, $|L\rangle$ and $|R\rangle$, and the basis of delocalized Hamiltonian eigenstates, which are the symmetric and antisymmetric linear combinations of the localized states, $\left|\phi^S\right\rangle = \left(|L\rangle + |R\rangle\right)/\sqrt{2}$ and $\left|\phi^A\right\rangle = \left(|L\rangle - |R\rangle\right)/\sqrt{2}$. The Hamiltonian eigenstates carry trivial time evolution as solutions of the time-independent Schrödinger equation and are therefore convenient for studying time dependence.

For our purposes, the lowest two NEO-CI vibronic states can be denoted $\left|\phi^S\right\rangle$ and $\left|\phi^A\right\rangle$ for the symmetric and antisymmetric proton wavefunctions, respectively (Figure 1). We

construct an initial wavefunction for propagation as an equally weighted linear combination of these two NEO-CI states to approximately localize the initial proton density in one of the wells. Analytically, given an initial wavefunction localized in the left well, the time-dependent probabilities of being localized in the left and right wells are given by

$$|c_L(t)|^2 = \cos^2\left(\frac{\Delta E t}{2\hbar}\right) \tag{7a}$$

$$|c_R(t)|^2 = \sin^2\left(\frac{\Delta E t}{2\hbar}\right) \tag{7b}$$

respectively, where ΔE is the energy difference between the Hamiltonian eigenstates in the absence of an applied field. Assuming the double-well potential is symmetric about the origin and the dipole moment of the solution localized in the left (right) well is D ($-D$), the time-dependent dipole moment is $D\cos\left(\frac{\Delta E t}{\hbar}\right)$.

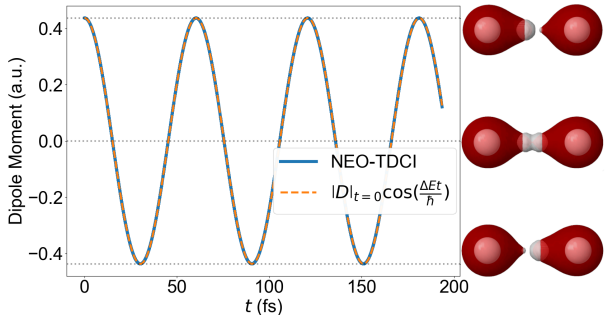

Figure 5: $HeHHe^+$ dipole moment from a NEO-TDCI simulation initialized with the proton approximately localized in a single well (i.e., near one of the He nuclei). Overlaid with the calculated dipole moment (solid blue line) is the analytical time-dependent dipole moment (dashed yellow line). The right hand plots are snapshots from the included movie showing the proton moving from one He to the other through a delocalized wavefunction characteristic of hydrogen tunneling.

In Figure 5, we plot the calculated dipole moment along the He–He axis for the NEO-TDCI simulation along with this analytic solution. The agreement between the calculated and analytic results is nearly exact, even across multiple oscillations of the proton between the two potential wells. As shown in the Supporting Information, even when utilizing the larger cc-pVDZ and PB5-F basis sets, the same level of agreement between the calculated

and analytic dipole moments is observed. Finally, we have included a video showing the time evolution of the protonic and electronic densities in white and red, respectively. The proton wavefunction oscillates between the two sides of the double-well potential via an intermediate delocalized solution characteristic of hydrogen tunneling. Snapshots illustrating this behavior are included in Figure 5. The electronic density also oscillates together with the protonic density in the middle region of the He–He axis.

Challenges remain for the application of the NEO-TDCI approach to larger, more realistic systems, both for calculating spectra and modeling hydrogen tunneling dynamics. Dynamic correlation beyond active space dynamic correlation must be included to accurately predict experimental transition energies.[42] Future work will explore multireference CI (MRCI) and complete active space perturbation theory (CASPT2) approaches within the NEO framework. For studying dynamics, active spaces must be designed to be capable of describing all relevant dynamics within the flexibility of a fixed active space. Although schemes exist for selecting active spaces to achieve ground state proton densities,[38] these schemes may not be appropriate for studying excited state properties, such as tunneling dynamics.

To summarize, we have implemented the NEO-TDCI approach and used it to calculate both the spectra and tunneling dynamics of $HeHHe^+$. We would like to emphasize that a single NEO-TDCI calculation can capture tunneling splittings, multiply excited states, and vibronic progressions in the NEO-TDCI spectra. All these features, which cannot be captured by single reference real-time methods, accurately reproduce the time-independent NEO-FCI spectra. The tunneling dynamics produced by the NEO-TDCI simulations illustrate the oscillation of the proton density from one side to the other via a delocalized, bilobal proton wavefunction indicative of hydrogen tunneling. These dynamics are in nearly exact agreement with the analytical solution for this model system. The NEO-TDCI approach is highly suitable for studying systems with strong electronic and/or protonic multiconfigurational character, dense vibronic spectra, and hydrogen tunneling dynamics, particularly in novel systems with proposed nuclear wavepacket interference.[54]

Acknowledgement

The development of NEO-CASCI methods in the Chronus Quantum computational software is supported by the Department of Energy in the Computational Chemical Science program (Grant No. DE-SC0023284). The software infrastructure, including NEO integrals and self-consistent-field, is supported by the Office of Advanced Cyberinfrastructure, National Science Foundation (Grant No. OAC-2103717 and OAC-2103902).

Supporting Information Available

The Supporting Information contains computational details for all real-time simulations, additional one dimensional slices of the proton and electron densities, calculations utilizing the larger basis set, and calculations for FHF^- (PDF) as well as a video showing the real-time dynamics of proton tunneling (MP4).

References

(1) Goings, J. J.; Lestrange, P. J.; Li, X. Real-time time-dependent electronic structure theory. *WIREs: Comput. Mol. Sci.* **2018**, *8*, e1341.

(2) Li, X.; Govind, N.; Isborn, C.; DePrince III, A. E.; Lopata, K. Real-time time-dependent electronic structure theory. *Chem. Rev.* **2020**, *120*, 9951–9993.

(3) Xu, J.; Carney, T. E.; Zhou, R.; Shepard, C.; Kanai, Y. Real-time time-dependent density functional theory for simulating nonequilibrium electron dynamics. *J. Am. Chem. Soc.* **2024**, *146*, 5011–5029.

(4) Tussupbayev, S.; Govind, N.; Lopata, K.; Cramer, C. J. Comparison of real-time and linear-response time-dependent density functional theories for molecular chromophores

ranging from sparse to high densities of states. *J. Chem. Theory Comput.* **2015**, *11*, 1102–1109.

(5) Thomas, I. Protonic structure of molecules. I. Ammonia molecules. *Phys. Rev.* **1969**, *185*, 90.

(6) Pettitt, B. A. Hartree-Fock theory of proton states in hydrides. *Chem. Phys. Lett.* **1986**, *130*, 399–402.

(7) Webb, S. P.; Iordanov, T.; Hammes-Schiffer, S. Multiconfigurational nuclear-electronic orbital approach: Incorporation of nuclear quantum effects in electronic structure calculations. *J. Chem. Phys.* **2002**, *117*, 4106–4118.

(8) Nakai, H.; Sodeyama, K. Many-body effects in nonadiabatic molecular theory for simultaneous determination of nuclear and electronic wave functions: *Ab initio* NOMO/MBPT and CC methods. *J. Chem. Phys.* **2003**, *118*, 1119–1127.

(9) Ishimoto, T.; Tachikawa, M.; Nagashima, U. Review of multicomponent molecular orbital method for direct treatment of nuclear quantum effect. *Int. J. Quantum Chem.* **2009**, *109*, 2677–2694.

(10) Pavošević, F.; Culpitt, T.; Hammes-Schiffer, S. Multicomponent quantum chemistry: Integrating electronic and nuclear quantum effects via the nuclear–electronic orbital method. *Chem. Rev.* **2020**, *120*, 4222–4253.

(11) Hammes-Schiffer, S. Nuclear–electronic orbital methods: Foundations and prospects. *J. Chem. Phys.* **2021**, *155*, 030901.

(12) Zhao, L.; Tao, Z.; Pavošević, F.; Wildman, A.; Hammes-Schiffer, S.; Li, X. Real-time time-dependent nuclear- electronic orbital approach: Dynamics beyond the Born–Oppenheimer approximation. *J. Phys. Chem. Lett.* **2020**, *11*, 4052–4058.

(13) Li, T. E.; Tao, Z.; Hammes-Schiffer, S. Semiclassical real-time nuclear-electronic orbital dynamics for molecular polaritons: Unified theory of electronic and vibrational strong couplings. *J. Chem. Theory Comput.* **2022**, *18*, 2774–2784.

(14) Zhao, L.; Wildman, A.; Pavosevic, F.; Tully, J. C.; Hammes-Schiffer, S.; Li, X. Excited state intramolecular proton transfer with nuclear-electronic orbital Ehrenfest dynamics. *J. Phys. Chem. Lett.* **2021**, *12*, 3497–3502.

(15) Chow, M.; Li, T. E.; Hammes-Schiffer, S. Nuclear–electronic orbital quantum mechanical/molecular mechanical real-time dynamics. *J. Phys. Chem. Lett.* **2023**, *14*, 9556–9562.

(16) Xu, J.; Zhou, R.; Blum, V.; Li, T. E.; Hammes-Schiffer, S.; Kanai, Y. First-principles approach for coupled quantum dynamics of electrons and protons in heterogeneous systems. *Phys. Rev. Lett.* **2023**, *131*, 238002.

(17) Li, T. E.; Hammes-Schiffer, S. Nuclear-electronic orbital quantum dynamics of plasmon-driven H2 photodissociation. *J. Am. Chem. Soc.* **2023**, *145*, 18210–18214.

(18) Runge, E.; Gross, E. K. Density-functional theory for time-dependent systems. *Phys. Rev. Lett.* **1984**, *52*, 997.

(19) Provorse, M. R.; Isborn, C. M. Electron dynamics with real-time time-dependent density functional theory. *Int. J. Quantum Chem.* **2016**, *116*, 739–749.

(20) Cohen, A. J.; Mori-Sánchez, P.; Yang, W. Challenges for density functional theory. *Chem. Rev.* **2012**, *112*, 289–320.

(21) Stein, T.; Kronik, L.; Baer, R. Reliable prediction of charge transfer excitations in molecular complexes using time-dependent density functional theory. *J. Am. Chem. Soc.* **2009**, *131*, 2818–2820.

(22) Rohringer, N.; Gordon, A.; Santra, R. Configuration-interaction-based time-dependent orbital approach for ab initio treatment of electronic dynamics in a strong optical laser field. *Phys. Rev. A* **2006**, *74*, 043420.

(23) Sato, T.; Ishikawa, K. L. Time-dependent complete-active-space self-consistent-field method for multielectron dynamics in intense laser fields. *Phys. Rev. A* **2013**, *88*, 023402.

(24) Klamroth, T. Laser-driven electron transfer through metal-insulator-metal contacts: Time-dependent configuration interaction singles calculations for a jellium model. *Phys. Rev. B* **2003**, *68*, 245421.

(25) Schlegel, H. B.; Smith, S. M.; Li, X. Electronic optical response of molecules in intense fields: Comparison of TD-HF, TD-CIS, and TD-CIS (D) approaches. *J. Chem. Phys.* **2007**, *126*, 244110.

(26) Krause, P.; Klamroth, T.; Saalfrank, P. Molecular response properties from explicitly time-dependent configuration interaction methods. *J. Chem. Phys.* **2007**, *127*, 034107.

(27) Luppi, E.; Head-Gordon, M. Computation of high-harmonic generation spectra of H2 and N2 in intense laser pulses using quantum chemistry methods and time-dependent density functional theory. *Mol. Phys.* **2012**, *110*, 909–923.

(28) White, A. F.; Heide, C. J.; Saalfrank, P.; Head-Gordon, M.; Luppi, E. Computation of high-harmonic generation spectra of the hydrogen molecule using time-dependent configuration-interaction. *Mol. Phys.* **2016**, *114*, 947–956.

(29) Lestrange, P. J.; Hoffmann, M. R.; Li, X. Time-dependent configuration interaction using the graphical unitary group approach: Nonlinear electric properties. *Adv. Quantum Chem.* **2018**, *76*, 295–313.

(30) Ulusoy, I. S.; Stewart, Z.; Wilson, A. K. The role of the CI expansion length in time-dependent studies. *J. Chem. Phys.* **2018**, *148*, 014107.

(31) Carlström, S.; Spanner, M.; Patchkovskii, S. General time-dependent configuration-interaction singles. I. Molecular case. *Phys. Rev. A* **2022**, *106*, 043104.

(32) Hochstuhl, D.; Bonitz, M. Time-dependent restricted-active-space configuration-interaction method for the photoionization of many-electron atoms. *Phys. Rev. A* **2012**, *86*, 053424.

(33) Bauch, S.; Sørensen, L. K.; Madsen, L. B. Time-dependent generalized-active-space configuration-interaction approach to photoionization dynamics of atoms and molecules. *Phys. Rev. A* **2014**, *90*, 062508.

(34) Wang, H.; Bokarev, S. I.; Aziz, S. G.; Kühn, O. Density matrix-based time-dependent configuration interaction approach to ultrafast spin-flip dynamics. *Mol. Phys.* **2017**, *115*, 1898–1907.

(35) Schriber, J. B.; Evangelista, F. A. Time dependent adaptive configuration interaction applied to attosecond charge migration. *J. Chem. Phys.* **2019**, *151*, 171102.

(36) Liu, H.; Jenkins, A. J.; Wildman, A.; Frisch, M. J.; Lipparini, F.; Mennucci, B.; Li, X. Time-dependent complete active space embedded in a polarizable force field. *J. Chem. Theory Comput.* **2019**, *15*, 1633–1641.

(37) Pak, M. V.; Hammes-Schiffer, S. Electron-proton correlation for hydrogen tunneling systems. *Phys. Rev. Lett.* **2004**, *92*, 103002.

(38) Fajen, O. J.; Brorsen, K. R. Multicomponent CASSCF revisited: Large active spaces are needed for qualitatively accurate protonic densities. *J. Chem. Theory Comput.* **2021**, *17*, 965–974.

(39) Yu, Q.; Hammes-Schiffer, S. Nuclear-electronic orbital multistate density functional theory. *J. Phys. Chem. Lett.* **2020**, *11*, 10106–10113.

(40) Dickinson, J. A.; Yu, Q.; Hammes-Schiffer, S. Generalized nuclear-electronic orbital multistate density functional theory for multiple proton transfer processes. *J. Phys. Chem. Lett.* **2023**, *14*, 6170–6178.

(41) Brorsen, K. R. Quantifying multireference character in multicomponent systems with heat-bath configuration interaction. *J. Chem. Theory Comput.* **2020**, *16*, 2379–2388.

(42) Alaal, N.; Brorsen, K. R. Multicomponent heat-bath configuration interaction with the perturbative correction for the calculation of protonic excited states. *J. Chem. Phys.* **2021**, *155*, 234107.

(43) Muolo, A.; Baiardi, A.; Feldmann, R.; Reiher, M. Nuclear-electronic all-particle density matrix renormalization group. *J. Chem. Phys.* **2020**, *152*, 204103.

(44) Feldmann, R.; Muolo, A.; Baiardi, A.; Reiher, M. Quantum proton effects from density matrix renormalization group calculations. *J. Chem. Theory Comput.* **2022**, *18*, 234–250.

(45) Blanes, S.; Casas, F.; Murua, A. Symplectic splitting operator methods for the time-dependent Schrödinger equation. *J. Chem. Phys.* **2006**, *124*, 234105.

(46) Peng, W.-T.; Fales, B. S.; Levine, B. G. Simulating electron dynamics of complex molecules with time-dependent complete active space configuration interaction. *J. Chem. Theory Comput.* **2018**, *14*, 4129–4138.

(47) Williams-Young, D. B.; Petrone, A.; Sun, S.; Stetina, T. F.; Lestrange, P.; Hoyer, C. E.; Nascimento, D. R.; Koulias, L.; Wildman, A.; Kasper, J. et al. The Chronus Quantum software package. *WIREs: Comput. Mol. Sci.* **2020**, *10*, e1436.

(48) Olsen, J.; Roos, B. O.; Jørgensen, P.; Jensen, H. J. A. Determinant based configuration interaction algorithms for complete and restricted configuration interaction spaces. *J. Chem. Phys.* **1988**, *89*, 2185–2192.

(49) Jmol development team Jmol. `http://jmol.sourceforge.net/`, Accessed 09-15-2023.

(50) Skone, J. H.; Pak, M. V.; Hammes-Schiffer, S. Nuclear-electronic orbital nonorthogonal configuration interaction approach. *J. Chem. Phys.* **2005**, *123*, 134108.

(51) Hehre, W. J.; Ditchfield, R.; Pople, J. A. Self—consistent molecular orbital methods. XII. Further extensions of Gaussian—type basis sets for use in molecular orbital studies of organic molecules. *J. Chem. Phys.* **1972**, *56*, 2257–2261.

(52) Yu, Q.; Pavošević, F.; Hammes-Schiffer, S. Development of nuclear basis sets for multicomponent quantum chemistry methods. *J. Chem. Phys.* **2020**, *152*, 244123.

(53) Dunning Jr, T. H. Gaussian basis sets for use in correlated molecular calculations. I. The atoms boron through neon and hydrogen. *J. Chem. Phys.* **1989**, *90*, 1007–1023.

(54) Zhang, X.; Schwarz, K. N.; Zhang, L.; Fassioli, F.; Fu, B.; Nguyen, L. Q.; Knowles, R. R.; Scholes, G. D. Interference of nuclear wavepackets in a pair of proton transfer reactions. *Proc. Natl. Acad. Sci. USA* **2022**, *119*, e2212114119.